Nanoscale Infrared Absorption Spectroscopy of Individual Nanoparticles Enabled by Scattering-Type Near-Field Microscopy

Johannes M. Stiegler,[†,▽] Yohannes Abate,[‡,§,#,▽] Antonija Cvitkovic,[⊥] Yaroslav E. Romanyuk,[‡,△] Andreas J. Huber,[⊥] Stephen R. Leone,[‡,§] and Rainer Hillenbrand[†,∥,*]

[†]Nanooptics Group, CIC nanoGUNE Consolider, Donostia—San Sebastián, Spain, [‡]Departments of Chemistry and Physics, University of California, Berkeley, California, United States, [§]Chemical Sciences Division, Lawrence Berkeley National Laboratory, Berkeley, California, United States, [⊥]Neaspec GmbH, Martinsried, Germany, and [∥]IKERBASQUE, Basque Foundation for Science, Bilbao, Spain. [#]Present address: Department of Physics and Astronomy, California State University Long Beach, California, United States. [△]Present address: Laboratory for Thin Films and Photovoltaics, Empa. Swiss Federal Laboratories for Materials Science and Technology, Dübendorf, Switzerland. [▽]These authors contributed equally to this work.

ABSTRACT Infrared absorption spectroscopy is a powerful and widely used tool for analyzing the chemical composition and structure of materials. Because of the diffraction limit, however, it cannot be applied for studying individual nanostructures. Here we demonstrate that the phase contrast in substrate-enhanced scattering-type scanning near-field optical microscopy (s-SNOM) provides a map of the infrared absorption spectrum of individual nanoparticles with nanometer-scale spatial resolution. We succeeded in the chemical identification of silicon nitride nanoislands with heights well below 10 nm, by infrared near-field fingerprint spectroscopy of the Si—N stretching bond. Employing a novel theoretical model, we show that the near-field phase spectra of small particles correlate well with their far-field absorption spectra. On the other hand, the spectral near-field contrast does not scale with the volume of the particles. We find a nearly linear scaling law, which we can attribute to the near-field coupling between the near-field probe and the substrate. Our results provide fundamental insights into the spectral near-field contrast of nanoparticles and clearly demonstrate the capability of s-SNOM for nanoscale chemical mapping based on local infrared absorption.

KEYWORDS: scattering-type near-field microscopy · infrared absorption spectroscopy · nanoparticles · phase contrast · chemical identification · nanoscale resolution

The analysis of chemical composition as well as structure is a major topic in chemical, physical, and biological sciences. A reliable and widely used tool for this analysis is infrared (IR) absorption spectroscopy. However, it normally cannot be applied to study individual nanoparticles and molecules, owing to the extremely small IR absorption cross sections and the diffraction-limited spatial resolution.

Scattering-type scanning near-field optical microscopy (s-SNOM)[1] is a powerful and versatile scanning probe technique, overcoming the diffraction limit in the infrared and terahertz spectral regime by several orders of magnitude.[2] s-SNOM is typically based on an atomic force microscope (AFM), where the sharp metallic probe tip is illuminated by a focused laser beam (Figure 1a). The tip functions as an IR antenna converting the illuminating radiation into a highly localized and enhanced near field at the tip apex.[2−5] Due to the IR near-field interaction between tip and sample, the tip-scattered radiation is modified in both its amplitude and its phase, depending on the local dielectric properties of the sample.[1] Interferometric detection (Figure 1b) of the backscattered light thus yields nanoscale-resolved IR amplitude and phase images, revealing the local, complex-valued, dielectric properties of the sample. From the near-field images the local structural properties,[6,7] the material composition,[2,8−12] and the free-carrier concentration[2,13−16] can be derived.

The sensitivity of s-SNOM can be improved by placing the sample of interest (*e.g.*, nanoparticles or thin films) on substrates with a high refractive index (*e.g.*, Si or Au) or with polaritonic properties (*e.g.*, SiC).[4,17] This sensitivity improvement can be explained by near-field coupling between tip and substrate, which enhances the field strength at the tip apex.[4,17−20] The tip—substrate configuration in s-SNOM—acting like a ground-plane antenna and referred to as substrate-enhanced s-SNOM[4,17]—has enabled the imaging of gold particles with sizes below 10 nm,[4,8] the spectral signature of thin polymer films[17] and the secondary structure of amyloid fibrils[21] supported by a gold substrate. The interpretation of the IR

* Address correspondence to r.hillenbrand@nanogune.eu.

Received for review May 13, 2011 and accepted July 19, 2011.

Published online July 19, 2011
10.1021/nn2017638

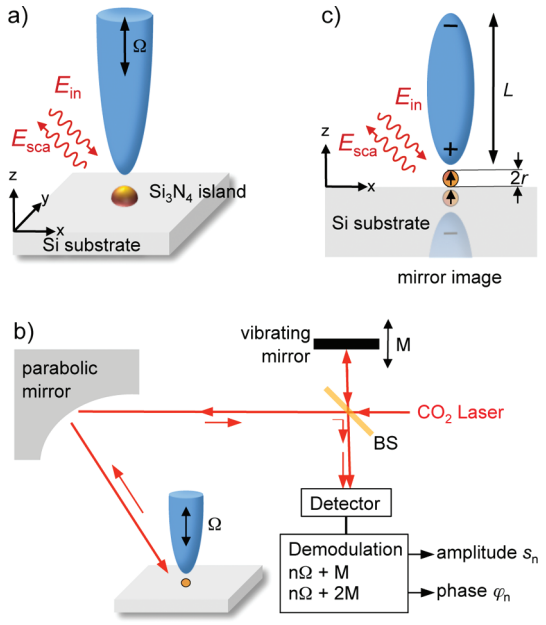

Figure 1. s-SNOM imaging of Si_3N_4 nanoparticles. (a) Near-field probing of Si_3N_4 nanoislands with an IR laser illuminating the scanning-probe tip, which is vibrating at frequency Ω. (b) Experimental setup. A Michelson interferometer is used for detecting the light scattered by the tip. BS labels the beam splitter of the interferometer. Pseudoheterodyne detection is performed by oscillating the reference mirror with frequency M. By demodulating the detector signal at nΩ + M and at nΩ + 2M, both amplitude s_n and phase φ_n are obtained. (c) Illustration of the finite-dipole model used for calculating the near-field response of single nanoparticles.

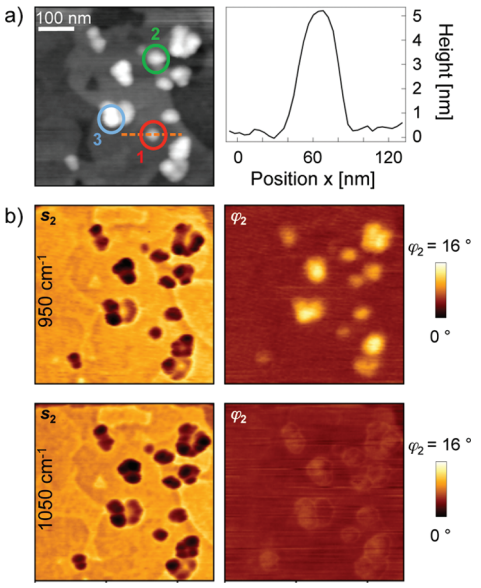

Figure 2. Experimental images of Si_3N_4 nanoislands. (a) Topography as well as (b) IR near-field amplitude s_2 and phase φ_2 at the two frequencies 950 and 1050 cm^{-1}. The line plot shows the height profile along the dashed orange line in the topography image. The numbered circles 1−3 mark the particles analyzed in Figures 3 and 4.

near-field spectra relies on theoretical modeling,[22,23] which still is a challenging task. An appropriate description of the tip-sample-substrate near-field interaction should take into account both the finite size of the sample and the tip, in order to explain size-dependent spectral near-field contrasts.[24]

Here we show that substrate-enhanced s-SNOM with interferometric detection allows for IR amplitude and phase resolved spectroscopy of the vibrational fingerprint of 5 nm high nanoislands. Particularly, we report near-field spectroscopy of the optical phonon polariton mode of individual silicon nitride (Si_3N_4) nanoislands associated with the Si−N stretching bond.[25] Using a novel theoretical framework based on the near-field interaction between tip, sample, and substrate, we perform a detailed analysis of the near-field amplitude and phase spectra and compare the results with calculated far-field absorption spectra.

RESULTS AND DISCUSSION

Near-field IR spectroscopic imaging was performed with a custom-made s-SNOM.[1] It is based on an AFM in which conventional Pt-coated Si-tips (apex radius $R \approx$ 20 nm) are illuminated by a focused CO_2 laser beam at frequencies between 890 and 1100 cm^{-1} (Figure 1a). Operating the AFM in tapping mode, the tip is vertically vibrating with an amplitude of about 20−30 nm at a frequency of $\Omega \approx$ 300 kHz. A Michelson interferometer (Figure 1b) is used to detect the tip-scattered light. Employing a pseudo-heterodyne detection scheme enables the simultaneous detection of both amplitude s and phase φ of the scattered field. Background signals are efficiently suppressed by demodulating the detector signal at the n-th harmonic $n \cdot \Omega$ of the tapping frequency.[26] In the present experiments second-harmonic demodulation (n = 2) was employed, yielding amplitude s_2 and phase φ_2 images simultaneously with topography.

Figure 2a shows a typical topography image and Figure 2b the simultaneously recorded IR amplitude s_2 and phase φ_2 images of the Si_3N_4 islands with heights ranging from 5 to 10 nm. The heights of the islands are directly measured from the topography image. Near-field amplitude s_2 and phase φ_2 images were recorded on and off the small-particle IR resonance of Si_3N_4 at 950 and 1050 cm^{-1}, respectively. In both amplitude images, the Si_3N_4 nanoislands appear darker than the substrate. Such a negative contrast has been also observed for Au[8] and InGaN[27] nanoparticles in previous s-SNOM studies.[27] Comparing the IR amplitude images at the two different frequencies, no significant change of the contrast between substrate and nanoislands is seen. The near-field phase images, however, exhibit a pronounced spectral contrast variation. In the phase image at 950 cm^{-1} we observe a clear contrast between the Si_3N_4 particles and the substrate, which nearly vanishes at 1050 cm^{-1}. Typically, a spectral phase contrast in s-SNOM reveals an absorption in the sample, for example caused by a vibrational resonance.[24,28]

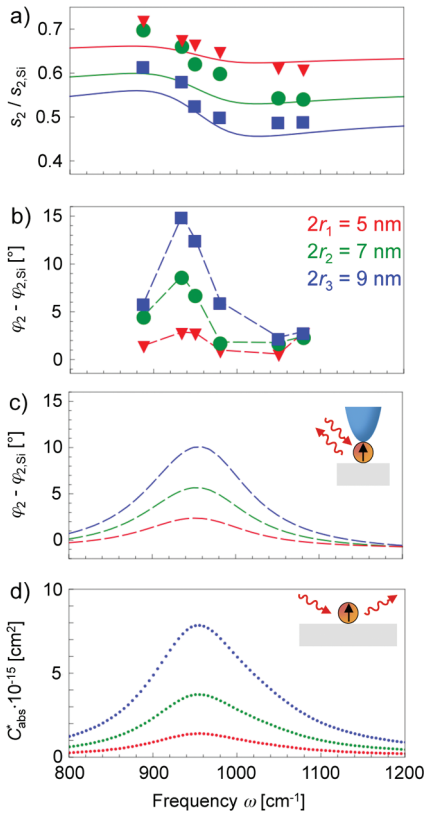

Figure 3. IR spectral characteristics of individual Si_3N_4 nanoparticles. (a) Near-field amplitude s_2. Symbols represent values obtained from particles 1−3 in Figure 2a. The solid lines display calculations based on the finite-dipole model (Figure 1c) and Si_3N_4 dielectric data taken from the literature.[31] (b) Experimental and (c) calculated near-field phase φ_2 of particles 1−3. In (a)−(c), the particles are located on a Si substrate and both the experimental and the calculated data are normalized to the IR near-field amplitude $s_{2,Si}$ and phase $\varphi_{2,Si}$ of the flat Si surface. (d) Calculated absorption cross-section of single Si_3N_4 nanoparticles on a Si substrate.

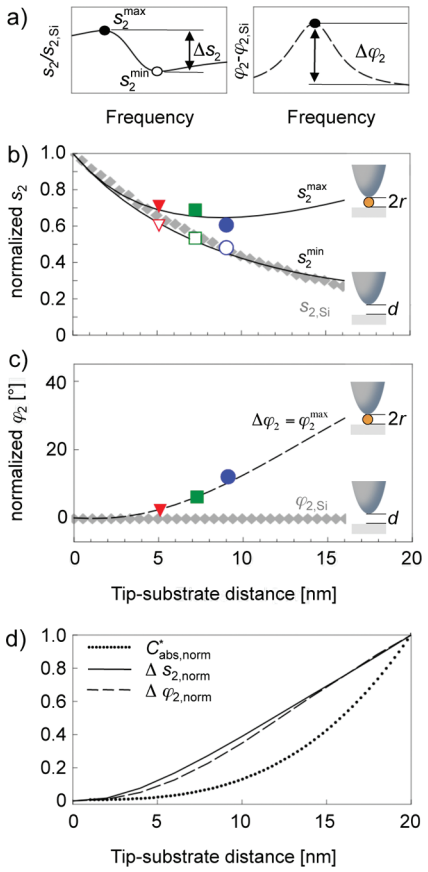

Figure 4. IR signals of single Si_3N_4 nanoparticles as a function of the particle diameter d. (a) Definition of spectral amplitude $\Delta s_2 = s_2^{max} - s_2^{min}$ and phase contrast $\Delta\varphi_2 = \varphi_2^{max}$. (b, c) Experimental (gray diamonds) near-field amplitude s_2 and phase φ_2 at 950 cm^{-1} as a function of distance d between tip and Si substrate. Filled and open symbols in (b) represent experimentally obtained s_2^{max} and s_2^{min} values, respectively, for particles 1−3 in Figure 2a, whereas solid black lines show theoretical s_2^{max} and s_2^{min} values, respectively, for an increasing particle diameter $2r$. Filled symbols in (c) represent φ_2^{max} values for particles 1−3 in Figure 2a, and the black dashed line represents the theoretical φ_2^{max} curve. All values have been normalized to the value taken on the Si substrate at d = 0. (d) Calculated absorption cross-section (dotted line), near-field amplitude contrast (solid line), and near-field phase contrast (dashed line), all normalized to the corresponding value of a 20 nm Si_3N_4 particle.

Thus, the spectral phase contrast of the Si_3N_4 nanoislands indicates that we map the vibrational resonance of the Si−N stretching bond.

To study the frequency-dependent near-field contrast between the Si_3N_4 nanoislands and the Si substrate in more detail, we imaged the sample at six different frequencies between 890 and 1100 cm^{-1}. Near-field spectra are obtained by measuring amplitude s_2 and phase φ_2 on top of individual Si_3N_4 nanoislands at the different frequencies. We evaluated three representative nanoislands with heights of 5, 7, and 9 nm (labeled 1−3 in Figure 2a). Experimental amplitude and phase spectra are shown as symbols in Figure 3a and b. For all three nanoislands, the amplitude s_2 spectra reveal only a weak signal decrease between 900 and 1000 cm^{-1}, which explains why in the amplitude images of Figure 2b the spectral amplitude contrast is barely visible. In the phase φ_2 spectra (Figure 3b) we find a peak with a maximum at 930 cm^{-1}. We furthermore find that both the spectral amplitude contrast Δs_2 (Figure 3a) and the spectral phase contrast $\Delta\varphi_2$ (Figure 3b) decrease with decreasing height of the nanoisland. The definitions of $\Delta s_2 = s_2^{max} - s_2^{min}$ and $\Delta\varphi_2 = \varphi_2^{max}$ are illustrated in Figure 4a.

To understand the s-SNOM amplitude and phase contrast of the nanoislands, we use a novel theoretical framework, which was developed to calculate the amplitude s_n and phase φ_n signals of particles smaller than the tip-apex (Figure 1c).[29] It is based on the finite-dipole model,[23] where the scattered field $E_{sca} = \sigma E_{in} = se^{i\varphi}E_{in}$—described by the complex-valued scattering coefficient σ—is derived from the near-field interaction between the illuminated tip and a flat semi-infinite substrate. The near-field probe is approximated by an isolated metal spheroid located in a uniform electric field. The spheroid is then reduced to a finite dipole p_0, which consists of the charges Q_0 and $-Q_0$, of which

only Q_0 (positioned closer to the sample surface) participates in the near-field interaction. Because of the interaction between Q_0 and the sample surface, an additional point charge Q_i is induced close to the spheroid focus, whereas the opposite charge $-Q_i$ is distributed along the spheroid. The charges Q_i and $-Q_i$ form a finite dipole p_i, which describes the scattering from the spheroid that is induced by its near-field interaction with the sample surface. The scattered field is obtained by calculating $E_{sca} \propto p_i E_{in}$. Assuming a sinusoidally varying tip−substrate distance at frequency Ω, the model yields the time course of the scattered field $E_{sca}(t)$. By Fourier transformation we subsequently obtain the n-th amplitude and phase coefficients, s_n and φ_n. To model the near-field signals of the Si_3N_4 nanoislands, we locate a Si_3N_4 sphere between the tip and the substrate. We assume a sphere diameter of $2r$, where $2r$ corresponds to the measured height d of the nanoislands. The polarizability of the sphere is given by $\alpha_{Sphere} = 4\pi r^3(\varepsilon(\omega) - 1)/(\varepsilon(\omega) + 2)$,[30] where $\varepsilon(\omega)$ represents the dielectric function of Si_3N_4. The finite probe dipole p_i is now calculated by considering the near-field interaction between the tip apex, the sphere, and the substrate, yielding the near-field amplitude $s_n(r)$ and phase $\varphi_n(r)$ signals of the particles as a function of the particle radius r. A detailed description of this model can be found in ref 29.

Using literature data for the dielectric function $\varepsilon(\omega)$ of Si_3N_4 from ref 31 we calculate near-field amplitude s_2 and phase φ_2 spectra for Si_3N_4 spheres with diameters of 5, 7, and 9 nm. The amplitude spectra (solid lines in Figure 3a) are in good agreement with the experimental data and clearly reproduce the amplitude decrease between 900 and 1000 cm^{-1}. These results reveal the typical s-SNOM amplitude spectra of a vibrational resonance, which has been derived earlier and shown for a PMMA[28] film and a tobacco mosaic virus.[24] We further find in Figure 3a that both the experimental and calculated s_2 signals increase with decreasing particle size, while the spectral amplitude contrast Δs_2 decreases. The increasing signal level is caused by an enhanced tip−substrate near-field coupling when the tip−substrate distance d is reduced.[4] The vanishing spectral contrast can be explained by the decreasing particle polarizability α_{Sphere} when the particle diameter $2r$ becomes smaller. We also find good agreement between the calculated (Figure 3c) and experimental (Figure 3b) phase spectra φ_2, showing a significant peak at 950 cm^{-1}, which decreases for smaller particle diameters. The small differences between experiment and theory can be explained by two main factors: (i) The Si_3N_4 islands have pyramidal shape, as described in the Methods section. In the calculation, however, we assume spherical particles with diameters corresponding to the heights measured from the topography image. (ii) The dielectric function of Si_3N_4 used for the calculations is taken from literature,[31] which may differ from the dielectric function of the Si_3N_4 nanoislands.

Interestingly, the near-field phase spectra resemble the absorption spectra of small particles. The correlation between near-field phase and far-field absorption spectra has been already pointed out earlier in ref 28, where calculated near-field phase and far-field absorption spectra of polymer bulk samples were compared. To establish this important correlation, particularly for nanoparticles, we calculate the far-field absorption cross-section of Si_3N_4 particles on a Si substrate. We assume an illumination polarization normal to the Si surface (*i.e.*, grazing incidence). Taking into account the influence of the substrate (coupling between particle dipole and its image dipole in the sample), we find for the Si_3N_4 particle a polarizability $\alpha^*_{Sphere} = \alpha_{Sphere}/[1 - (\alpha_{Sphere}(\varepsilon - 1)(\varepsilon + 1)^{-1})/(16\pi r^3)]$, yielding an absorption cross-section $C^*_{abs} = k\,\mathrm{Im}[\alpha^*_{Sphere}]$.[32] In Figure 3d, we show C^*_{abs} for 5, 7, and 9 nm Si_3N_4 particles. Comparing the near-field phase signals φ_2 and the far-field absorption cross-section C^*_{abs}, we find that both exhibit the same qualitative spectral behavior. This clearly shows that the phase of the tip-scattered light reveals the absorption characteristic of small particles, despite the complex near-field interaction between tip, particle, and substrate.

We can understand the relation between the far-field absorption cross-section C^*_{abs} of the particles and the near-field phase φ_2 by considering that the scattering coefficient $\sigma = se^{i\varphi}$ is given by $\sigma = \sigma_{t\text{-}s} + \sigma_{p,eff}$, where $\sigma_{t\text{-}s}$ is the scattering coefficient of the tip−substrate configuration without a sample (particle) and $\sigma_{p,eff}$ the additional contribution when a sample (particle) is located between tip and substrate. Assuming that $s_{t\text{-}s} \gg s_{p,eff}$, we obtain $\varphi = \arg[\sigma] \approx \mathrm{Im}[\sigma_{p,eff}]/s_{t\text{-}s}$. With $\sigma_{p,eff} = k^2\alpha_{p,eff}$ ($\alpha_{p,eff}$ being the effective polarizability of the particle when located between tip and substrate) and the general relation $C_{abs} = k\,\mathrm{Im}[\alpha]$ for small scatterers, we find that the phase of the scattered light is proportional to the effective absorption cross-section of the particle in the tip−substrate system, $\varphi \propto \mathrm{Im}[\alpha_{p,eff}] \propto C_{abs,eff}$. Comparing now parts c and d of Figure 3, we find that the phase spectra φ_2 exhibit a good agreement with C^*_{abs}, the latter being the absorption cross-section of the particle on the substrate alone, *i.e.*, in the absence of the tip. We thus conclude that the presence of the tip does not significantly modify the spectral signature of the particles.

To explore the sensitivity of s-SNOM, we study the spectral IR amplitude and phase contrasts (Figure 4a) as a function of the particle height. To this end, we show in Figure 4b the measured Si_3N_4 amplitude signals s_2^{max} (filled symbols) and s_2^{min} (open symbols) as a function of the particle height $2r$. For comparison, we also show the measured amplitude signal $s_{2,Si}$ above the Si as a function of the tip−substrate distance

d (gray diamonds). Two important observations are made. (i) For a given particle height $2r$, the amplitude s_2^{max} is larger than the signal $s_{2,Si}$ measured for a tip–substrate separation $d = 2r$. This is because the presence of the Si_3N_4 particle enhances the near-field interaction between tip and substrate.[15] (ii) For any tip sample separation d, the amplitude signals $s_2^{max}(d)$ on top of the Si_3N_4 particles are smaller than the amplitude signal $s_{2,Si}(d = 0)$ measured directly at the Si surface. This explains why in the amplitude images in Figure 2b the particles appear darker than the substrate (note that the oscillating AFM tip is following the sample surface). In Figure 4c we observe that the measured phase contrast $\Delta\varphi_2$ (filled symbols) increases with an increasing particle height, while the measured phase signal $\varphi_{2,Si}(d)$ on the Si substrate (gray diamonds) is constant, *i.e.*, independent of the tip–substrate distance d. This explains why the particles in the phase images at 950 cm^{-1} (Figure 2b) appear brighter than the substrate. Calculations using the finite-dipole model (solid and dashed black lines, respectively) clearly reproduce the experimental data in Figure 4b and c. We note that the increasing contrast is valid only for particles smaller than the apex radius R, which is the approximation underlying the model. The calculations also show that for particles with $2r < 5$ nm both the amplitude and phase contrast vanish, thus challenging their experimental detection. The reason for the decreasing contrast of both the amplitude and phase contrast is the decreasing particle polarizability when the particle becomes smaller. We note that the particle size where Δs_2 and $\Delta\varphi_2$ vanish is determined by the size and the optical properties of the probing tip. Thus using sharper tips with radii below 10 nm and with optimized antenna properties[33,34] of the tip–substrate configuration, the detection limit could be pushed further towards smaller particles.

In Figure 4d we compare the calculated spectral near-field amplitude and phase contrasts, Δs_2 and $\Delta\varphi_2$, with the far-field absorption C^*_{abs}. We observe that both the amplitude and phase contrast show a nearly linear increase with the particle diameter $2r$ between 5 and 20 nm, while the absorption cross-section C^*_{abs} scales cubically. This beneficial scaling law for IR near-field spectroscopy can be attributed to the increased near-field coupling between tip and substrate when the particle size (*i.e.*, the gap width $d = 2r$) is decreased. The enhanced near-field coupling provides higher fields for polarizing the reduced amount of particle matter. Thus it partially compensates the decreasing particle polarizability.[4]

CONCLUSIONS

We have demonstrated the near-field detection of the IR spectrum of nanoislands with heights below 10 nm by using an interferometric s-SNOM. The results show that near-field IR phase spectra of small particles exhibit a significant correlation to the far-field absorption. It can be understood by the fact that the dielectric properties of a material are complex-valued numbers,[32] where the real part describes the refractive and the imaginary part the absorptive properties. The latter gives rise to a phase shift of the scattered light with respect to the incident light, which can be easily recorded by interferometric detection in s-SNOM. Thus, interferometric s-SNOM has the capability to map the IR absorption of materials with nanoscale spatial resolution. By engineering the antenna function of metal probe tips and by reducing the tip apex below 10 nm,[35] we envision s-SNOM to become a valuable tool for IR absorption spectroscopy of even single macromolecules.

METHODS

The Si_3N_4 particles were prepared by first annealing Si(111) wafers in an ultra-high-vacuum chamber with a base pressure of 1×10^{-7} Pa. A Si wafer was cleaned by three separate sonications in acetone, 2-propanol, and methanol, dried in a nitrogen flow, and transferred into the vacuum chamber. The Si wafer was first heated to 800 °C and then flashed three times for 60 s at 1020 °C. Under these conditions the surface silicon oxide layer gradually decomposes, resulting in self-assembled silicon nanoislands.[36] Next, the sample was exposed to nitrogen plasma generated with a radio frequency plasma source. *In situ* Auger spectroscopy (not shown) confirmed the formation of silicon nitride, presumably the Si_3N_4 phase, without the incorporation of impurities such as carbon and oxygen. Finally, the nitrified sample was flash heated again for 10 min at 1020 °C. This procedure yields Si_3N_4 pyramidal-shaped nanoislands with a base radius between 10 and 20 nm and varying heights below 10 nm at a density of 5×10^8 cm^{-2}.

Acknowledgment. We thank N. Ocelic (Neaspec GmbH, Martinsried) and P. S. Carney (University of Illinois at Urbana–Champaign) for discussions. This work was financially supported by the National Project MAT2009-08398 from the Spanish Ministerio de Ciencia e Innovacion. A.C. acknowledges the KMU-Innovationsofensive-NanoChance Project from the BMBF for financial support. The Berkeley authors gratefully acknowledge Department of Energy financial support for Y.A. and supplies, by the Director, Office of Science, Office of Basic Energy Sciences, U.S. Department of Energy under Contract No. DE-AC02-05CH11231 through the Division of Materials Research. Y.E.R. acknowledges prospective researcher fellowship no. PBEL2-112358 from the Swiss National Science Foundation and partial support by the U.S. National Science Foundation Engineering Research Center grant for Extreme Ultraviolet Science and Technology no. EEC-0310717.

REFERENCES AND NOTES

1. Keilmann, F.; Hillenbrand, R. Near-Field Microscopy by Elastic Light Scattering from a Tip. *Philos. Trans. R. Soc. A* **2004**, *362*, 787–805.
2. Huber, A. J.; Keilmann, F.; Wittborn, J.; Aizpurua, J.; Hillenbrand, R. Terahertz Near-Field Nanoscopy of Mobile

Carriers in Single Semiconductor Nanodevices. *Nano Lett.* **2008**, *8*, 3766–3770.
3. Sanchez, E. J.; Novotny, L.; Xie, X. S. Near-Field Fluorescence Microscopy Based on Two-Photon Excitation with Metal Tips. *Phys. Rev. Lett.* **1999**, *82*, 4014–4017.
4. Cvitkovic, A.; Ocelic, N.; Aizpurua, J.; Guckenberger, R.; Hillenbrand, R. Infrared Imaging of Single Nanoparticles Via Strong Field Enhancement in a Scanning Nanogap. *Phys. Rev. Lett.* **2006**, *97*, 060801.
5. Brehm, M.; Schliesser, A.; Cajko, F.; Tsukerman, I.; Keilmann, F. Antenna-Mediated Back-Scattering Efficiency in Infrared Near-Field Microscopy. *Opt. Express* **2008**, *16*, 11203–11215.
6. Huber, A. J.; Ziegler, A.; Kock, T.; Hillenbrand, R. Infrared Nanoscopy of Strained Semiconductors. *Nat. Nanotechnol.* **2009**, *4*, 153–157.
7. Kehr, S. C.; Cebula, M.; Mieth, O.; Haertling, T.; Seidel, J.; Grafstroem, S.; Eng, L. M.; Winnerl, S.; Stehr, D.; Helm, M. Anisotropy Contrast in Phonon-Enhanced Apertureless Near-Field Microscopy Using a Free-Electron Laser. *Phys. Rev. Lett.* **2008**, *100*, 256403.
8. Cvitkovic, A.; Ocelic, N.; Hillenbrand, R. Material-Specific Infrared Recognition of Single Sub-10 nm Particles by Substrate-Enhanced Scattering-Type Near-Field Microscopy. *Nano Lett.* **2007**, *7*, 3177–3181.
9. Akhremitchev, B. B.; Sun, Y.; Stebounova, L.; Walker, G. C. Monolayer-Sensitive Infrared Imaging of DNA Stripes Using Apertureless Near-Field Microscopy. *Langmuir* **2002**, *18*, 5325–5328.
10. Arsov, Z.; Quaroni, L.; Havenith, M. Nanoscale Depth Resolution in Scanning Near-Field Infrared Microscopy. *Opt. Express* **2008**, *16*, 7453–7459.
11. Ogawa, Y.; Minami, F.; Abate, Y.; Leone, S. R. Nanometer-Scale Dielectric Constant of Ge Quantum Dots Using Apertureless Near-Field Scanning Optical Microscopy. *Appl. Phys. Lett.* **2010**, *96*, 063107.
12. Raschke, M. B.; Molina, L.; Elsaesser, T.; Kim, D. H.; Knoll, W.; Hinrichs, K. Apertureless Near-Field Vibrational Imaging of Block-Copolymer Nanostructures with Ultrahigh Spatial Resolution. *ChemPhysChem* **2005**, *6*, 2197–2203.
13. Stiegler, J. M.; Huber, A. J.; Diedenhofen, S. L.; Gomez Rivas, J.; Algra, R. E.; Bakkers, E. P. A. M.; Hillenbrand, R. Nanoscale Free-Carrier Profiling of Individual Semiconductor Nanowires by Infrared Near-Field Nanoscopy. *Nano Lett.* **2010**, *10*, 1387–1392.
14. Knoll, B.; Keilmann, F. Infrared Conductivity Mapping for Nanoelectronics. *Appl. Phys. Lett.* **2000**, *77*, 3980–3982.
15. Samson, J.-S.; Wollny, G.; Brundermann, E.; Bergner, A.; Hecker, A.; Schwaab, G.; Dirk Wieck, A.; Havenith, M. Setup of a Scanning Near Field Infrared Microscope (SNIM): Imaging of Sub-Surface Nano-Structures in Gallium-Doped Silicon. *Phys. Chem. Chem. Phys.* **2006**, *8*, 753–758.
16. Qazilbash, M. M.; *et al*. Mott Transition in VO_2 Revealed by Infrared Spectroscopy and Nano-Imaging. *Science* **2007**, *318*, 1750–1753.
17. Aizpurua, J.; Taubner, T.; García de Abajo, F. J.; Brehm, M.; Hillenbrand, R. Substrate-Enhanced Infrared Near-Field Spectroscopy. *Opt. Express* **2008**, *16*, 1529–1545.
18. Neacsu, C. C.; Dreyer, J.; Behr, N.; Raschke, M. Scanning-Probe Raman Spectroscopy with Single-Molecule Sensitivity. *Phys. Rev. B* **2006**, *73*, 193406.
19. Pettinger, B.; Ren, B.; Picardi, G.; Schuster, R.; Ertl, G. Nanoscale Probing of Adsorbed Species by Tip-Enhanced Raman Spectroscopy. *Phys. Rev. Lett.* **2004**, *92*, 096101.
20. Deckert-Gaudig, T.; Bailo, E.; Deckert, V. Tip-Enhanced Raman Scattering (TERS) of Oxidised Glutathione on an Ultraflat Gold Nanoplate. *Phys. Chem. Chem. Phys.* **2009**, *11*, 7360–7362.
21. Paulite, M.; Fakhraai, Z.; Li, I. T. S.; Gunari, N.; Tanur, A. E.; Walker, G. C. Imaging Secondary Structure of Individual Amyloid Fibrils of a b_2-Microglobulin Fragment Using Near-Field Infrared Spectroscopy. *J. Am. Chem. Soc.* **2011**, *133*, 7376–7383.
22. Knoll, B.; Keilmann, F. Enhanced Dielectric Contrast in Scattering-Type Scanning Near-Field Optical Microscopy. *Opt. Commun.* **2000**, *182*, 321–328.
23. Cvitkovic, A.; Ocelic, N.; Hillenbrand, R. Analytical Model for Quantitative Prediction of Material Contrasts in Scattering-Type Near-Field Optical Microscopy. *Opt. Express* **2007**, *15*, 8550–8565.
24. Brehm, M.; Taubner, T.; Hillenbrand, R.; Keilmann, F. Infrared Spectroscopic Mapping of Single Nanoparticles and Viruses at Nanoscale Resolution. *Nano Lett.* **2006**, *6*, 1307–1310.
25. Parsons, G. N.; Souk, J. H.; Batey, J. Low Hydrogen Content Stoichiometric Silicon Nitride Films Deposited by Plasma-Enhanced Chemical Vapor Deposition. *J. Appl. Phys.* **1991**, *70*, 1553–1560.
26. Ocelic, N.; Huber, A.; Hillenbrand, R. Pseudoheterodyne Detection for Background-Free Near-Field Spectroscopy. *Appl. Phys. Lett.* **2006**, *89*, 101124.
27. Kim, Z. H.; Ahn, S.-H.; Liu, B.; Leone, S. R. Nanometer-Scale Dielectric Imaging of Semiconductor Nanoparticles: Size-Dependent Dipolar Coupling and Contrast Reversal. *Nano Lett.* **2007**, *7*, 2258–2262.
28. Taubner, T.; Hillenbrand, R.; Keilmann, F. Nanoscale Polymer Recognition by Spectral Signature in Scattering Infrared Near-Field Microscopy. *Appl. Phys. Lett.* **2004**, *85*, 5064–5066.
29. Cvitkovic, A. Substrate-Enhanced Scattering-Type Scanning Near-Field Infrared Microscopy of Nanoparticles. Ph.D. Thesis, Technische Universität München, München, 2009.
30. Jackson, J. D. *Classical Electrodynamics*, 3rd ed.; Wiley: New York, 1999.
31. Brendel, R.; Bormann, D. An Infrared Dielectric Function Model for Amorphous Solids. *J. Appl. Phys.* **1992**, *71*, 1–6.
32. Bohren, C. F.; Huffmann, D. R. *Absorption and Scattering of Light by Small Particles*; Wiley: New York, 1983.
33. Weber-Bargioni, A.; Schwartzberg, A.; Cornaglia, M.; Ismach, A.; Urban, J. J.; Pang, Y.; Gordon, R.; Bokor, J.; Salmeron, M. B.; Ogletree, D. F.; *et al.* Hyperspectral Nanoscale Imaging on Dielectric Substrates with Coaxial Optical Antenna Scan Probes. *Nano Lett.* **2011**, *11*, 1201–1207.
34. Zou, Y.; Steinvurzel, P.; Yang, T.; Crozier, K. B. Surface Plasmon Resonances of Optical Antenna Atomic Force Microscope Tips. *Appl. Phys. Lett.* **2009**, *94*, 171107.
35. De Angelis, F.; Das, G.; Candeloro, P.; Patrini, M.; Galli, M.; Bek, A.; Lazzarino, M.; Maksymov, I.; Liberale, C.; Andreani, L. C.; *et al*. Nanoscale Chemical Mapping Using Three-Dimensional Adiabatic Compression of Surface Plasmon Polaritons. *Nat. Nanotechnol.* **2010**, *5*, 67–72.
36. Palermo, V.; Jones, D. Self-Organised Growth of Silicon Structures on Silicon During Oxide Desorption. *Mater. Sci. Eng., B* **2002**, *88*, 220–224.